Title	Road condition recognition using 24 GHz automotive radar
Author(s)	Viikari, Ville; Varpula, Timo; Kantanen, Mikko
Citation	IEEE Transactions on Intelligent Transportation Systems vol. 10(2009):4, pp. 639-648
Date	2009
URL	http://dx.doi.org/10.1109/TITS.2009.2026307
Rights	Copyright © [2009] IEEE. Reprinted from IEEE Transactions on Intelligent Transportation Systems vol. 10(2009):4, pp. 639-648.

VTT
http://www.vtt.fi
P.O. box 1000
FI-02044 VTT
Finland

Road-Condition Recognition Using 24-GHz Automotive Radar

Ville V. Viikari, *Associate Member, IEEE*, Timo Varpula, and Mikko Kantanen

***Abstract*—This paper studies 24-GHz automotive radar technology for detecting low-friction spots caused by water, ice, or snow on asphalt. The backscattering properties of asphalt in different conditions are studied in both laboratory and field experiments. In addition, the effect of water on the backscattering properties of asphalt is studied with a surface scattering model. The results suggest that low-friction spots could be detected with a radar by comparing backscattered signals at different polarizations. The requirements for the radar are considered, and a 24-GHz radar for road-condition recognition is found to be feasible.**

***Index Terms*—Radar applications, road vehicle radar, scattering.**

I. Introduction

AUTOMOTIVE radars are becoming standard equipment in premium cars, and they are also expected to become common in medium and lower class cars. The radars are expected to increase safety and to facilitate driving. Commercially available radars are either for blind-spot detection (BSD) or for automatic cruise control (ACC) [1]. BSD systems ease certain maneuvering such as lane changing, whereas ACC systems adjust the vehicle speed according to the preceding vehicle.

Currently, two frequency bands are allocated for automotive radars in Europe: the 22–24-GHz band for short-range (30-m) radars [2] and the 76–77-GHz band for long-range (150-m) radars [3]. The third band, i.e., 77–81 GHz, is being currently allocated by the European Telecommunications Standards Institute (ETSI) for short-range (30-m) collision-warning automotive radars [4].

Automotive radars could also possibly be used to detect road conditions such as low friction due to water, ice, or snow on the road. Currently, infrared optical sensors and some mechanical devices are used to monitor road conditions [5]. These systems are either unsuitable or too expensive for ordinary cars. Their detection range is also limited in the forward direction; in fact, it is nil in some cases. Multipurpose radar sensors offer clear benefits: The total number of sensors in a vehicle is not increased, yielding cost benefits. The detection range of a radar is potentially substantial.

Several studies on using automotive radars for road-condition recognition are reported. Bistatic (the transmitter and the receiver are in different locations) scattering measurements from different road surfaces under laboratory conditions are reported at 76 [6] and 24 GHz [7]. The scattering from different road surfaces is measured with a coherent polarimetric radar. Road conditions are then recognized from the eigenvalues of the Stokes or Mueller matrix [8]. The measurement results at both frequencies indicate that it is possible to distinguish between two concrete roads with different roughness. The authors state that moisture on the road can be detected at 76 GHz. The results at 24 GHz show that water, ice, snow, and rime on the road change the road's scattering properties.

Kees and Detlefsen report a bistatic radar system operating at 61 GHz that recognizes road conditions [9]. The radar system is located under the car chassis, and it is able to transmit and receive at both linear polarizations. The system coherently measures all four polarization combinations, and the road condition is recognized by comparing the amplitudes and/or phases between responses at different polarizations. Measurements with a prototype radar revealed that the system is able to distinguish between asphalt and cobblestone road pavements.

Finkele has reported a bistatic radar operating at 76 GHz that is capable of detecting ice layers on the road surface [10]. This fully polarimetric radar measures the specular reflection from the road and utilizes the polarization properties of the reflected wave to detect ice. The operation principle is verified with simulations and measurements made in the laboratory and under real traffic conditions.

Hetzner has measured different road conditions using an active bistatic radar and a passive radiometer operating at 35 and 90 GHz [11]. In his experiments, the radiometer was found to be more suitable for road-condition recognition.

Magerl *et al.* report a fixed 2.45-GHz road surveillance radar capable of detecting weather-induced road conditions [12]. Both the transmitter and the receiver are located 3 m high on opposite sides of the road. According to the results with the prototype radar, the system is capable of measuring water-layer thickness and water salinity, as well as detecting the snow layer on the road.

Automotive radars are also proposed for other novel applications such as detecting lane and pavement boundaries and advance paths in [13] and [14], respectively. A vehicle and guard rail-detection system based on combined radar and vision data is reported in [15]. In addition, a radar system capable of avoiding collisions by autonomous steering is presented in [16].

Manuscript received June 6, 2008; revised October 29, 2008 and January 22, 2009. First published July 21, 2009; current version published December 3, 2009. This work was supported in part by the European Union Commission under Contract FP6-IST-2004-4-027006 of the FRICTION project. The Associate Editor for this paper was R. Goudy.

The authors are with the VTT Technical Research Centre of Finland, 02044 Espoo, Finland (e-mail: ville.viikari@vtt.fi; timo.varpula@vtt.fi; mikko.kantanen@vtt.fi).

Color versions of one or more of the figures in this paper are available online at http://ieeexplore.ieee.org.

Digital Object Identifier 10.1109/TITS.2009.2026307

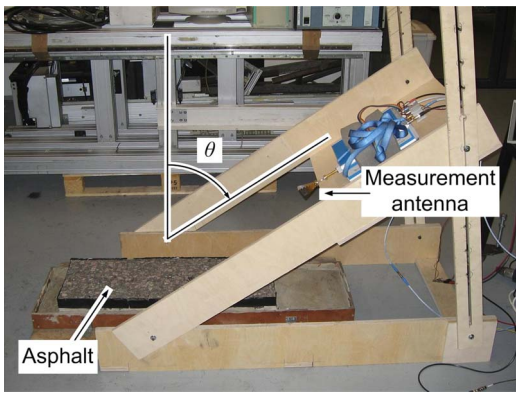

Fig. 1. Measurement set up. The measurement horn antenna, which is mounted on the rotating arm, points toward the asphalt sample placed on the floor.

In addition to the previously mentioned scientific publications, there are several patents and patent applications on automotive radars for road-condition recognition [17]–[19].

In this paper, we study the capabilities of a 24-GHz forward-looking monostatic (the transmitter and the receiver are in the same location) radar as a detector of low-friction spots on asphalt. This paper is organized as follows. Section II discusses laboratory experiments on the backscattering properties of dry, wet, and icy asphalt. Section III presents field experiments on the backscattering properties of dry, wet, icy, and snowy asphalt. A rough-surface scattering model is used to study the effect of surface parameters on backscattering in Section IV. Section V discusses the radar requirements for detecting road conditions, and Section VI concludes the paper.

II. Laboratory Experiments

Backscattering properties of dry, wet, and icy asphalt at 24 and 77 GHz are studied under laboratory conditions in [20]. For convenience, the measurement procedure is briefly described in the following with the selected measurement results at 24 GHz.

A. Measurement Setup

Monostatic backscattering from an asphalt sample is measured with a network analyzer (HP 8510) and a horn antenna (Flann Microwave Mod 20240-20-AA with 37-mm aperture size in the E-field direction and 52 mm in the H-field direction) mounted on a rotating arm to allow for the backscattering measurements at incidence angles from 0° to 80°. The incidence angle increment of 5° was selected as a good compromise between describing the backscattering properties of asphalt in sufficient detail and providing a short enough measurement time to prevent the melting of icy asphalt during the tests in the room-temperature laboratory. The measurement distance is 46 cm, fulfilling the generally required far-field criterion of $R \geq 2D^2/\lambda$, where D is the largest dimension of the radar antenna, and λ is the wavelength. Fig. 1 shows a photograph of the measurement setup: a 295 × 800 mm asphalt sample (stone mastic asphalt 16) is taken from a Finnish road with an average traffic flow of approximately 8000 vehicles/day. Because the sample is taken after the winter season, tires with studs, which are commonly used in Finland, have eroded the bitumen from the asphalt such that the rock filling is exposed. An ice layer of 1–2 mm was made by first cooling the asphalt sample with liquid nitrogen (−196 °C) and then watering it. The temperature of the ice remained between −5 °C and −15 °C during the experiments.

B. Power Calibration

The backscattered power was calibrated by measuring the normal reflection from a metal plate. The reflected power from a metal plate is attenuated according to the Friis free-space formula

$$\frac{P_r}{P_t} = G^2 \left(\frac{\lambda}{4\pi r}\right)^2 \tag{1}$$

where $r = 2R_m$ is the two-way signal path length (with R_m being the one-way path length to the metal plate), P_t is the transmitted power, P_r is the received power, G is the antenna gain, and λ is the wavelength. The ratio between the received and the transmitted power is proportional to square of the reflected voltage

$$|S_{11,m}|^2 \sim \frac{P_r}{P_t} \Rightarrow |S_{11,m}|^2 = xG^2 \left(\frac{\lambda}{8\pi R_m}\right)^2 \tag{2}$$

where x is a constant. The radar cross section of the sample is

$$\sigma_s = \frac{P_r}{P_t} \frac{(4\pi)^3 R_s^4}{G^2 \lambda^2} \tag{3}$$

where R_s is the distance to the sample. Equation (3) can be written as

$$\sigma_s = \frac{|S_{11,s}|^2}{x} \frac{(4\pi)^3 R_s^4}{G^2 \lambda^2} \tag{4}$$

where $S_{11,s}$ is the measured reflection coefficient from the sample. Solving x from (2) and substituting it into (4) gives

$$\sigma_s = \frac{|S_{11,s}|^2}{|S_{11,m}|^2} \frac{\pi R_s^4}{R_m^2}. \tag{5}$$

The backscattered signal from a rough surface such as asphalt is a superposition of several weak signals produced by small irregularities on the surface. As these irregularities are often randomly distributed over a surface, the backscattered signal also randomly varies from one part of the surface to another. Therefore, it is meaningful to consider only the expectation value of the backscattered signal, which is denoted as $\langle\sigma\rangle$.

A road is an area-extensive target: Its effective target size (and, thus, also its radar cross section) depends on the illuminated surface area. Such targets are characterized in terms of the scattering coefficient, which defines the average radar cross section $\langle\sigma\rangle$ over illuminated surface area A_0 [21]

$$\sigma_0 = \frac{\langle\sigma\rangle}{A_0}. \tag{6}$$

The illuminated surface area is limited in the vertical direction by either the pulse length $c\tau$ or the vertical beamwidth θ_v

of the antenna, depending on which one is smaller. In the horizontal direction, the illuminated area is limited by the horizontal beamwidth θ_h of the radar antenna. The illuminated area is

$$A_0 = R_s \min\left\{\theta_h \frac{c\tau}{2}\sec(\pi/2-\phi), R_s\theta_v\right\} \tag{7}$$

where R_s is the distance to the (center of the) illuminated sample, c is the speed of light, ϕ is the incidence angle with respect to the surface normal, and the $\min\{\}$ operator selects the smallest value. Combining (5)–(7) gives the calibrated scattering coefficient of the sample

$$\sigma_0 = \frac{|S_{11,s}|^2}{|S_{11,m}|^2}\frac{\pi R_s^3}{R_m^2 \min\left\{\theta_h \frac{c\tau}{2}\sec(\pi/2-\phi), R_s\theta_v\right\}}. \tag{8}$$

The backscattering coefficients are defined for different polarizations. In the following, the backscattering coefficient is defined as σ_{pp}, where the first subindex refers to the polarization (h stands for horizontal and v for vertical) of the transmitted signal, and the second index refers to that of the received signal.

C. Signal Processing

To obtain reflections from the asphalt sample only, a time-gating procedure was employed. This way, the unwanted signals caused by reflections due to the impedance mismatch of the antenna and by reflections from the laboratory are eliminated. In time gating, the measured frequency response (18–26.5 GHz) is transformed into the time domain via Fourier transform. The time response is filtered with a gate function and then transformed back into the frequency domain to obtain the gated frequency response.

As the backscattering coefficient is defined as the statistical expectation value, several measurements on different (uncorrelated) samples should be performed to reliably obtain it. However, repeating the measurement several times with different asphalt samples is too laborious and time consuming. Therefore, the expectation of the backscattered signal is obtained here by averaging over a frequency band under assumptions that the average backscattering remains constant in the frequency band and that backscattering at different frequencies is uncorrelated.

D. Results

The measured backscattering coefficients at different incidence angles for dry, wet, and icy asphalt at 24 GHz are shown in Figs. 2 (for vv-polarization) and 3 (for hh-polarization).

Water on asphalt seems to increase the backscattering coefficient close to the normal incident, compared with dry asphalt. At larger incidence angles, water slightly increases the backscattering at vertical polarization, whereas it decreases backscattering at horizontal polarization. Ice does not change the backscattering coefficient at normal incidence but increases it at both polarizations at larger incidence angles, compared with dry asphalt.

In practice, the absolute value of the backscattering coefficient is not a suitable quantity for identifying water or ice on asphalt. First, absolute backscattering coefficient measurements are challenging with automotive radars since the target distance and weather conditions affect the backscattered signal. In addition, the incidence angle and the asphalt type, which are usually unknown parameters, also affect the backscattered signal. The effect of these unknown parameters is eliminated by computing ratios of backscattered signals for different polarizations. The ratios of backscattering coefficients at vv- and hh-polarizations $(\sigma_{\mathrm{vv}}/\sigma_{\mathrm{hh}})$ are shown in Fig. 4.

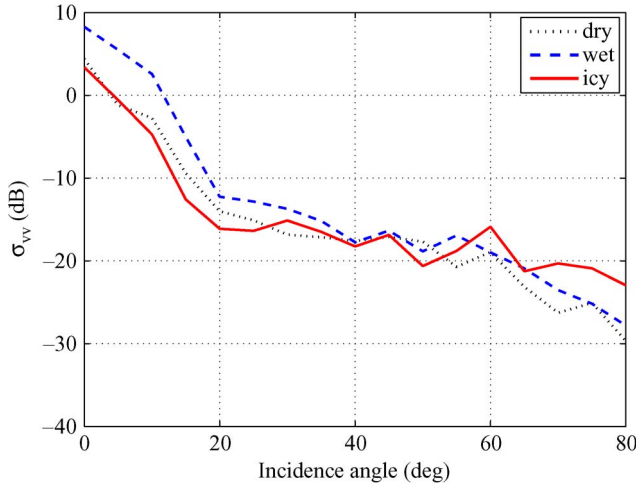

Fig. 2. Measured backscattering coefficient for (dotted line) dry, (dashed line) wet, and (solid line) icy asphalt at vv-polarization at 24 GHz.

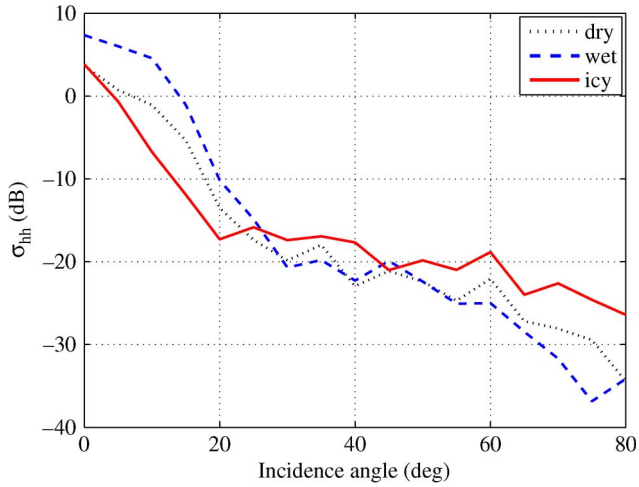

Fig. 3. Measured backscattering coefficient for (dotted line) dry, (dashed line) wet, and (solid line) icy asphalt at hh-polarization at 24 GHz.

Water does not have any effect on the ratio $\sigma_{\mathrm{vv}}/\sigma_{\mathrm{hh}}$ at small incidence angles, whereas at large incidence angles $(50°$–$80°)$, it is about 4 dB higher than that for dry asphalt. On the other hand, ice clearly increases $\sigma_{\mathrm{vv}}/\sigma_{\mathrm{hh}}$ at small incidence angles but slightly decreases the ratio at large incidence angles. The average decrease at large incidence angles is approximately 1 dB, even though a slight increase occurs at 70°. This is most likely caused by the reflections due to a nonideal measurement setup. However, these results suggest that water and ice change the backscattering properties of the asphalt in such a way that they could be identified by comparing the ratio $\sigma_{\mathrm{vv}}/\sigma_{\mathrm{hh}}$ at large incidence angles.

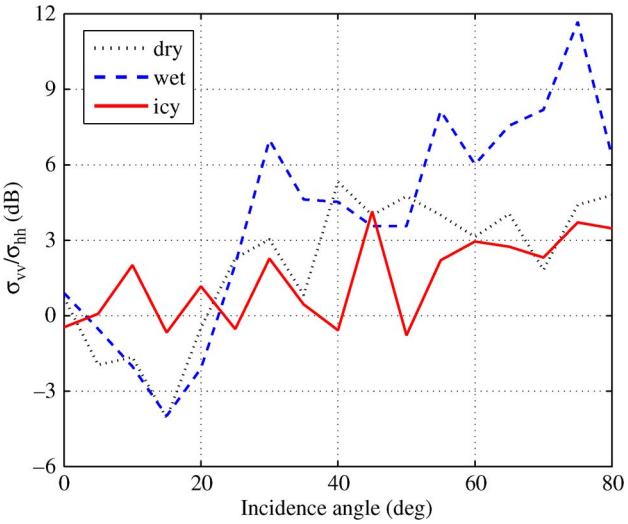

Fig. 4. Ratio between the backscattering coefficients at vv- and hh-polarizations at 24 GHz.

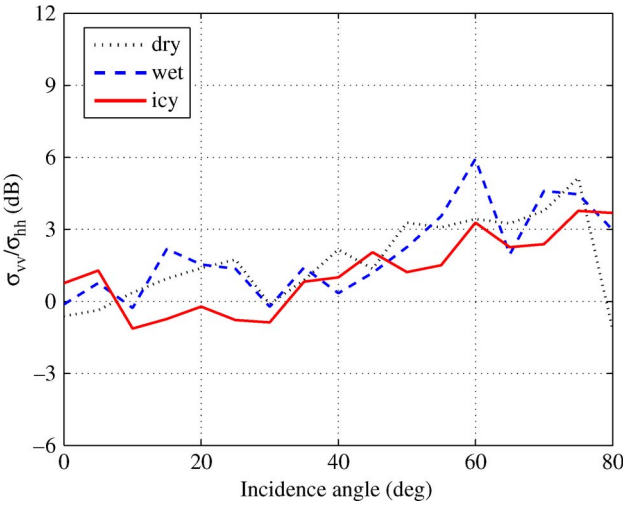

Fig. 5. Ratio between the backscattering coefficients at vv- and hh-polarizations at 77 GHz.

The laboratory experiments were also performed at 77 GHz, but the results at this frequency were not as promising as those at 24 GHz. The ratios of backscattering coefficients at 77 GHz at vv- and hh-polarizations $(\sigma_{\mathrm{vv}}/\sigma_{\mathrm{hh}})$ are shown in Fig. 5.

III. Field Experiments

The promising results from the laboratory experiments motivated us to study the 24-GHz road-condition recognition radar concept in two field experiment campaigns. The backscattering properties of icy and snowy asphalt were studied in the first measurement campaign during the winter, and the backscattering properties of wet asphalt were studied in the second campaign during the summer.

A. Measurement Setup for Winter Experiments

Test tracks, each having a different road condition, were prepared on a cast-off runway of Ivalo Airport, Finland. The road conditions studied were dry, icy, and snowy asphalt. The asphalt was slurry sealed with 8-mm rock filling, and it was quite smooth, as compared with normal asphalt-coated roads, as it was only slightly eroded. Ice and snow were removed from the asphalt using chemicals that are used to keep runways clear. These chemicals were brushed off from the asphalt, but it is possible that the asphalt contained some residuals that might have a small effect on its electrical properties.

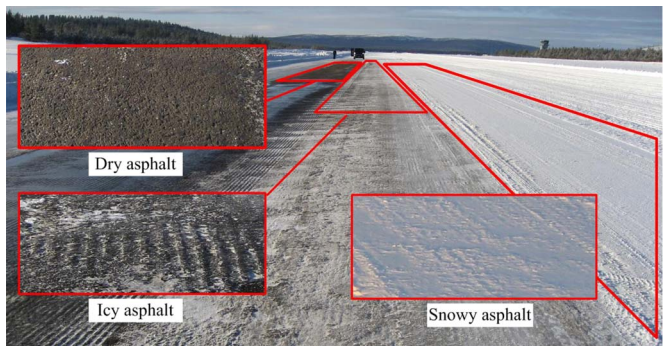

Fig. 6. Test tracks with different road conditions.

The icy part of the track had an approximately 5-cm ice layer. The ice surface was planed with a road grader used for plane icy roads, particularly in northern Finland. The grader produced about 1-cm-deep and 3-cm-wide grooves on the ice surface. The grooves were parallel to the driving direction, i.e., to the pointing direction of the radar.

The snow layer was approximately 10 cm thick, and it was stamped using a special stamping machine designed to produce road conditions similar to snowy roads in typical traffic situations.

Test tracks with different road conditions were at least 50 m long and 4 m wide. The test tracks, with close-ups of different road surfaces, are shown in Fig. 6.

The same equipment and measurement procedure were used as in the laboratory experiments. The measurement equipment was installed in the boot space of a van. The power was generated with an aggregate and delivered to the network analyzer through an uninterruptible power supply unit. The exhaust of the aggregate was transmitted out from the van with an extended exhaust pipe. The boot space of the van was heated up with an electric heater in an attempt to maintain the room temperature required by the network analyzer. The measurement antennas were aligned to point to the track from the opened back door of the van. The aperture of the opened back door was thermally isolated with a sheet of cellular plastic. The test van with the measurement equipment is shown in Fig. 7.

The measurement antennas were located approximately 1 m above the road surface. The backscattering from the test tracks was measured at 65° incidence with respect to the normal of the road surface. This incidence angle was chosen as a compromise between the detection range and the backscattered signal level and, thus, the measurement accuracy as well.

In these experiments, the backscattering measurements of each road condition were repeated five times to average the results. The measurement setup was not power calibrated because the objective of these measurements was not to calculate

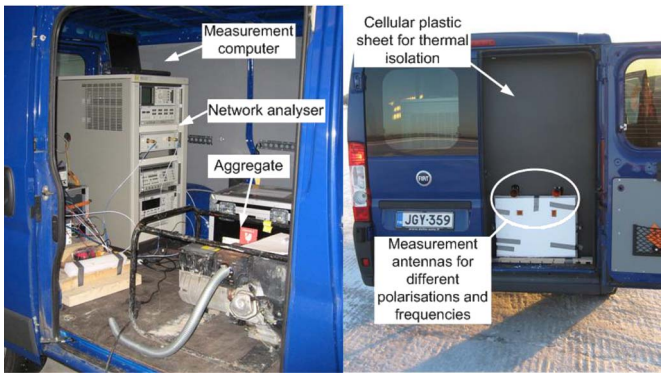

Fig. 7. Test van equipped with measurement equipment. (Left) Network analyzer, measurement computer, and the aggregate that were placed in the boot place of the van. (Right) Measurement antennas that pointed backward from the back door of the van.

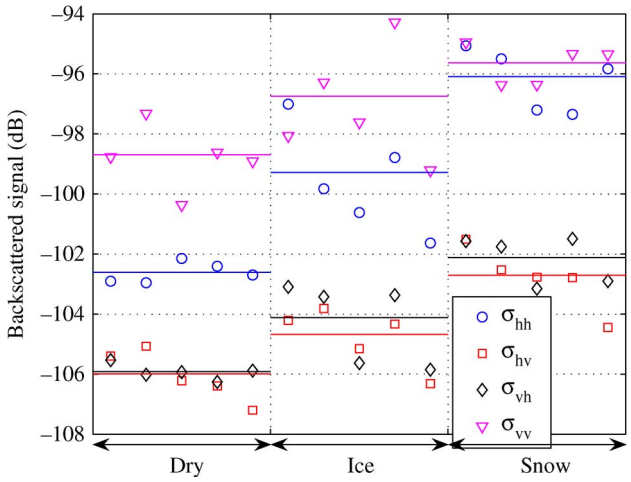

Fig. 8. Measured backscattering of dry, icy, and snowy asphalt at different polarizations. Single measurements are represented with markers, and solid lines are averaged values over respective road conditions and polarizations.

the absolute backscattering coefficients but to study how the ratio between backscattering at different polarizations changes with different road conditions. The road surface temperature was -10 °C to -15 °C during the experiments.

B. Measurement Setup for Summer Experiments

The backscattering properties of wet asphalt were studied in field experiments conducted in a test track located in Nokia, Finland. The measurement setup was similar to that used in the winter experiments. However, the measurement horns were located closer to the road surface (at 0.6-m height), and a power calibration was performed with a metal plate to obtain the absolute backscattering coefficients. The asphalt used for experiments was eroded by tires with studs.

C. Results

The measured backscattering of dry, icy, and snowy asphalt at different polarizations is shown in Fig. 8. The markers represent single measurements, and solid lines represent averages over values for respective road conditions and polarizations. The measured backscattering of dry and wet asphalt at different polarizations is shown in Fig. 9. Figs. 10 and 11 show the ratios of backscattering for different polarizations.

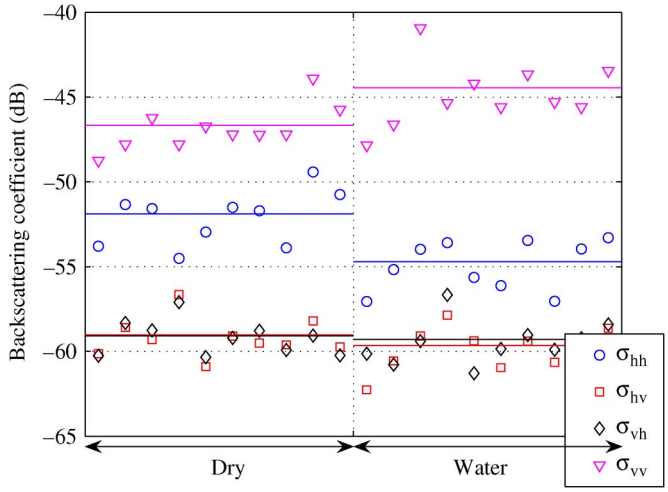

Fig. 9. Measured backscattering of dry and wet asphalt at different polarizations. Single measurements are represented with markers, and solid lines are averaged values over respective road conditions and polarizations.

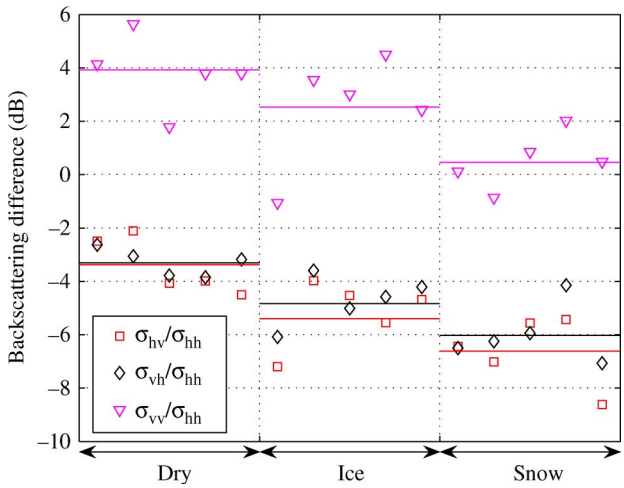

Fig. 10. Backscattering from dry, icy, and snowy asphalt at different polarizations normalized to that at vv-polarization. Single measurements are represented with markers, and solid lines are averaged values over respective road conditions and polarizations.

The data in Fig. 8 show that ice increases the backscattering at all polarizations from 2 to 3.5 dB, compared with dry asphalt. This result is in agreement with the laboratory experiment, where ice increased the backscattering at 65° incidence by 2–3 dB. As compared to icy asphalt, snow further increases the backscattering by 1–3.5 dB.

According to the reciprocity theorem, backscattering at hv-polarization is equal to that at vh-polarization. This seems to hold in these measurements, although the backscattering at vh-polarization is slightly larger than that at hv-polarization. This result gives an indication for the uncertainty and repeatability of the experiments.

Water increases the backscattering at horizontal polarization and decreases it at vertical polarization, compared with dry asphalt (see Fig. 9). This result is also in good agreement with the results from the laboratory tests.

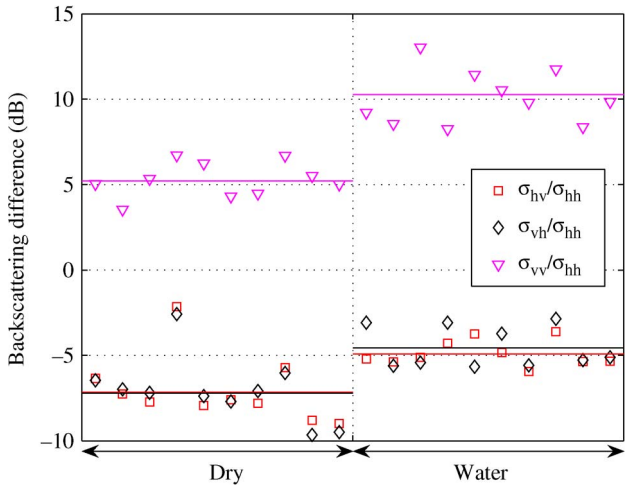

Fig. 11. Backscattering from dry and wet asphalt at different polarizations normalized to that at vv-polarization. Single measurements are represented with markers, and solid lines are averaged values over respective road conditions and polarizations.

As discussed earlier, it is more favorable to use ratios of different polarizations to detect road conditions. Fig. 10 shows that ice decreases ratios $\sigma_{\rm vv}/\sigma_{\rm hh}$, $\sigma_{\rm vh}/\sigma_{\rm hh}$, and $\sigma_{\rm hv}/\sigma_{\rm hh}$ by 1–1.5 dB, compared with dry asphalt. Snow seems to further decrease the ratios by 1–2 dB. On the contrary, water seems to increase ratio $\sigma_{\rm vv}/\sigma_{\rm hh}$ by approximately 5 dB, as seen in Fig. 11. According to these results, it is possible to detect water, ice, and snow on asphalt with a 24-GHz radar at 65° incidence angle. The variations between adjacent measurements on the same road condition, however, are so large that averaging is clearly required to reliably identify different road conditions. In an actual radar sensor that is capable of directly measuring these ratios, the variation is expected to be substantially smaller. In addition, computational methods such as clustering could be applied to enhance the identification reliability.

To compare both automotive radar bands for road-condition detection, the field experiments were also performed at 77 GHz. According to these experiments, a 24-GHz frequency seems to be better for road-condition recognition.

IV. Surface Scattering Modeling

The backscattering of asphalt is modeled to relate target parameters to its backscattering properties. The small-perturbation model, which was used for surface modeling, assumes homogenous target material. Contrary to water, ice and snow are low-loss materials at 24 GHz. When there is ice or snow on the asphalt, the radar signal experiences a layered structure. Therefore, the small-perturbation model could be used only for dry and wet asphalt.

A. Small-Perturbation Model

The small-perturbation model is used to model backscattering from a rough surface [21]. In this model, it is assumed that the target is of homogenous material and that the dimensions of the roughness are low, compared with the free-space wavelength. The backscattering coefficients are calculated from the following equations:

$$\gamma^0_{\rm pp} = \frac{k^2}{2} e^{-2k_z^2\gamma^2} \sum_{n=1}^{\infty} \left|I^n_{\rm pp}\right| \frac{W^{(n)}(-2k_x)}{n!} \tag{9}$$

$$I^n_{\rm pp} = (2k_z\gamma)^n f_{\rm pp} e\left(-k_z^2\gamma^2\right) + \frac{(k_z\gamma)^n\left[F_{\rm pp}(-k_x) + F_{\rm pp}(k_x)\right]}{2} \tag{10}$$

$$f_{\rm vv} = \frac{2R_{\rm hh}}{\cos\phi} \tag{11}$$

$$f_{\rm hh} = -\frac{2R_{\rm vv}}{\cos\phi} \tag{12}$$

$$F_{\rm vv}(-k_x) + F_{\rm vv}(k_x) = \frac{2\sin^2\phi(1+R_{\rm vv})^2}{\cos\phi}\left[\left(1-\frac{1}{\varepsilon_r}\right) + \frac{\mu_r\varepsilon_r - \sin^2\phi - \varepsilon_r\cos^2\phi}{\varepsilon_r^2\cos^2\phi}\right] \tag{13}$$

$$F_{\rm hh}(-k_x) + F_{\rm hh}(k_x) = \frac{2\sin^2\phi(1+R_{\rm hh})^2}{\cos\phi}\left[\left(1-\frac{1}{\mu_r}\right) + \frac{\mu_r\varepsilon_r - \sin^2\phi - \mu_r\cos^2\phi}{\mu_r^2\cos^2\phi}\right] \tag{14}$$

$$R_{\rm hh} = \frac{\varepsilon_r\cos\phi - \sqrt{\mu_r\varepsilon_r - \sin^2\phi}}{\varepsilon_r\cos\phi + \sqrt{\mu_r\varepsilon_r - \sin^2\phi}} \tag{15}$$

$$R_{\rm vv} = \frac{\mu_r\cos\phi - \sqrt{\mu_r\varepsilon_r - \sin^2\phi}}{\mu_r\cos\phi + \sqrt{\mu_r\varepsilon_r - \sin^2\phi}} \tag{16}$$

where $k_z = k\cos\phi$, $k_x = k\sin\phi$, $k = (2\pi/\lambda)$ is the wavenumber, ϕ is the incidence angle with respect to the normal of the surface, γ is the root-mean-square height of the surface slope, ε_r and μ_r are the relative permittivity and permeability of the target, subindices pp refer to the polarization (hh or vv), and $W^{(n)}(-2k_x)$ is the Fourier transform of the nth power of the surface correlation coefficient. Assuming that the surface shape is Gaussian correlated and that it has two scale roughnesses, which are not correlated, we then have

$$W^{(n)}(K) = \sum_{m=0}^{n} \frac{n!a^{n-m}b^m}{(n-m)!m!} \frac{L_e^2}{2} e^{-\frac{(KL_e)^2}{4}} \tag{17}$$

where $a = \gamma_1^2/\gamma$, $b = \gamma_2^2/\gamma$, γ_1^2 and γ_2^2 are the variances of the two scale slope heights, and γ^2 is the total variance of the slope height. The reference plane is chosen such that γ has zero mean. The square of the equivalent correlation length L is given as

$$L^2 = \frac{L_1^2L_2^2}{(n-m)L_2^2 + mL_1^2} \tag{18}$$

where L_1 and L_2 are the correlation lengths of the two scale roughnesses. The model is valid only for small- and medium-scale surface roughness. For the validity of the small-perturbation model, it is usually required that

$$(k\gamma)(kL) < 1.2\sqrt{\varepsilon_r} \tag{19}$$

for a surface with permittivity ε_r.

TABLE I
PARAMETERS GIVING THE BEST FIT BETWEEN THE LABORATORY MEASUREMENTS AND THE MODEL

	Wet asphalt ($\varepsilon_r = 33$)
γ_1 (mm)	0.6545
L_1 (mm)	14.1840
γ_2 (mm)	0.2018
L_2 (mm)	3.7632

B. Model Fitting to the Measurements

As asphalt surface statistics, slope heights γ_1^2 and γ_2^2 and correlation lengths L_1 and L_2 are not directly available; the model is fitted to the laboratory measurement results. The surface parameters are chosen to minimize

$$\int |\sigma_{\mathrm{meas,vv}}(\phi) - \sigma_{\mathrm{model,vv}}(\phi)| + |\sigma_{\mathrm{meas,hh}}(\phi) - \sigma_{\mathrm{model,hh}}(\phi)|\, d\phi \quad (20)$$

where the measured σ_{meas} and modeled σ_{model} backscattering coefficients are given in decibels.

References [22] and [23] announce that the dielectric constant of asphalt is 2.6 at microwave frequencies. This value is used in the model for dry asphalt. According to the model presented in [24], the relative permittivity of 20 °C water is $33 - j36$ at 24 GHz, resulting into a skin depth of 0.77 mm. Because the water-layer thickness in the experiments was substantially higher than the skin depth, the relative permittivity of wet asphalt can be taken to be the same as that of the water. In this model, the relative permittivity of water is set to 33.

C. Modeled Backscattering

The surface parameters providing the best fit between the model and the laboratory measurement results from wet asphalt are listed in Table I.

The modeled backscattering coefficients from wet asphalt with the measured ones are shown in Fig. 12.

The model is used to study how surface parameters $(\varepsilon_r, \gamma_1, L_1, \gamma_2, L_2)$ affect the ratio $\sigma_{\mathrm{vv}}/\sigma_{\mathrm{hh}}$. Fig. 13 shows the ratio at different relative permittivities when other parameters correspond to those presented in Table I. Fig. 14 shows the same ratio at different values of γ_1 and L_1 when $\varepsilon_r = 33$. The effect of parameters γ_2 and L_2 is shown in Fig. 15.

Fig. 13 reveals that the ratio $\sigma_{\mathrm{vv}}/\sigma_{\mathrm{hh}}$ increases with the relative permittivity of the target. In this example, $\sigma_{\mathrm{vv}}/\sigma_{\mathrm{hh}}$ is increased by 17 dB at 70° incidence when the relative permittivity is increased from 3 to 33. As shown in Fig. 14, $\sigma_{\mathrm{vv}}/\sigma_{\mathrm{hh}}$ is not changed much when surface parameters γ_1 and L_1 are halved or doubled. When parameters γ_2 and L_2 are doubled from their original values, the ratio is decreased by 10 dB at large incidence angles, as shown in Fig. 15. However, within the range of used surface parameter values, the relative permittivity seems to be the most dominant parameter affecting $\sigma_{\mathrm{vv}}/\sigma_{\mathrm{hh}}$. This analysis indicates that water on asphalt affects the backscattering ratio much more significantly than the variations in asphalt properties. Thus, both theory and experiments

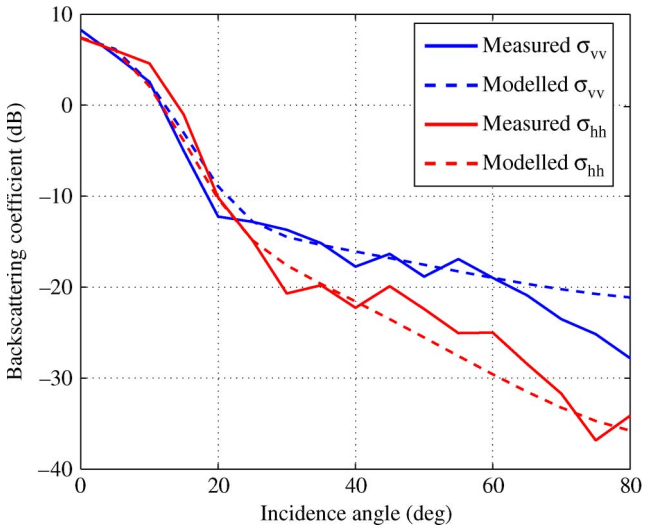

Fig. 12. Modeled backscattering coefficient from wet asphalt with the measured ones (under laboratory conditions).

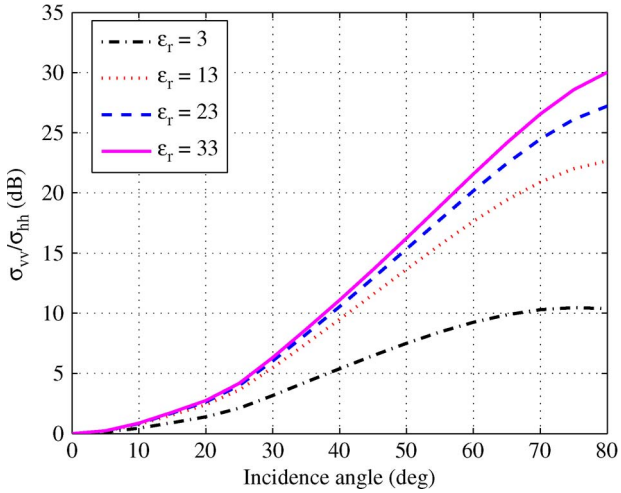

Fig. 13. Ratio between backscattering at vv- and hh-polarization at different values of relative permittivity.

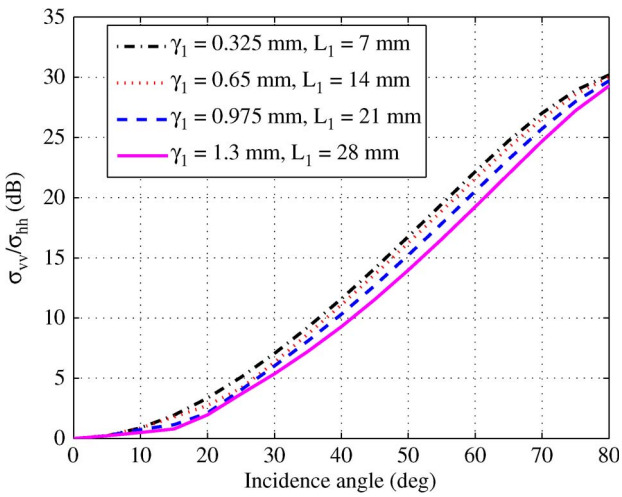

Fig. 14. Ratio between backscattering at vv- and hh-polarization at different values of γ_1 and L_1.

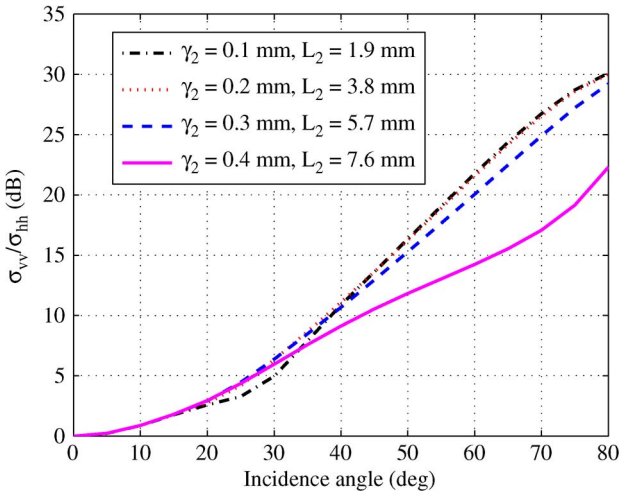

Fig. 15. Ratio between backscattering at vv- and hh-polarization at different values of γ_2 and L_2.

support the idea that water on asphalt can be detected with a 24-GHz radar with large incidence.

V. Requirements for the Radar

To be able to recognize different road conditions, the radar should be able to measure backscattering at different polarizations. Commercial automotive radar sensors, which operate only at single polarization, could be modified to operate at several polarizations by adding a dual-polarized antenna with a switch in the transmitter or the receiver side or both. A dual-polarized radar sensor that is suitable for automotive applications is described in [25].

When using a radar sensor for multiple purposes such as for road-condition recognition and for collision warning, a switchable antenna is required such that the radar beam can be switched between the road surface and the direction of motion of the vehicle. When using a short-range radar with a low-gain (and, thus, broad main beam) antenna, it might be possible to align the antenna such that it simultaneously sees both the road surface and further objects.

In the following, let us calculate the power budget for a 24-GHz short-range radar recognizing road conditions. Substituting (6) and (7) into the radar equation (3) gives the received power (at large incidence angles)

$$P_r = \frac{P_t G^2 \lambda^2 \sigma_0}{(4\pi R)^3} \cdot \frac{c\tau\theta_h}{2} \sec(\pi/2 - \phi). \tag{21}$$

A 24-GHz short-range automotive radar is presented in [26] with the following parameters: pulsewidth $\tau = 400$ ps, peak power $P_t = 6$ dBm, and equivalent isotropically radiated power, which is defined as a product of transmitted power and antenna gain, equal to 20 dBm. This gives an antenna gain of 14 dBi. Assuming a square aperture for the antenna, the beamwidth is approximately $\theta_h = 40^\circ$ at 24 GHz. Let us further assume that the radar is located 0.5 m above the ground and that the incidence angle is $\phi = 75^\circ$, resulting in a target distance of $R = 1.9$ m. According to the field experiments during the summer, the scattering coefficients may be -55 dB at the lowest. The noise floor of the receiver is given by

TABLE II
Estimated Power Budget

Transmitted power	$P_t = 6$ dBm
Antenna gain	$G = 14$ dBi
Wavelength at 24 GHz	$\lambda = 12.5$ mm
Distance to the illuminated area	$R = 1.9$ m
Scattering coefficient	$\sigma_0 = -55$ dB
Pulse width	$\tau = 400$ ps
Horizontal beam width of the antenna	$\theta_h = 40^\circ$
Incidence angle	$\phi = 75^\circ$
Received power	$P_r = -104.5$ dBm
Antenna temperature	$T_a = 270$ K
Receiver noise temperature	$T_a = 1160$ K
Noise bandwidth	$B = 9$ kHz
Noise floor	$P_n = -127.5$ dBm
Signal-to-noise – ratio	14 dB

$$P_n = k(T_r + T_a)B \tag{22}$$

where k is the Boltzmann constant, T_r is the noise temperature of the receiver, T_a is the noise temperature of the antenna, and B is the noise bandwidth. In the case of a frequency-modulated continuous-wave radar architecture, the noise bandwidth is limited by the Doppler frequency caused by the movement of the vehicle. Assuming a maximum vehicle speed of 200 km/h, the Doppler shift at 24 GHz is 9 kHz. Further assuming an antenna temperature of 270 K and a receiver noise temperature of 1160 K (corresponding to a 7-dB noise figure), the receiver noise floor is at -127.5 dBm, giving a 14-dB signal-to-noise ratio; see Table II. Thus, this estimation indicates that a 24-GHz short-range automotive radar for road-condition recognition seems to be feasible.

VI. Conclusion

This paper has studied the use of a 24-GHz automotive radar to detect low-friction spots caused by water, ice, or snow on asphalt. The backscattering properties of dry, wet, and icy asphalt have been studied in laboratory conditions, and the backscattering properties of dry, wet, icy, and snowy asphalt have been studied with field experiments. In addition, the effect of water on the backscattering properties of asphalt has been studied with a rough-surface scattering model.

The measurement of backscattering ratios for different polarizations turned out to be the best method to detect low-friction spots. This kind of differential measurement enables the elimination or reduction of the effects of most unknown parameters such as measurement distance, asphalt properties, weather conditions, etc., which affect absolute backscattering measurements.

Backscattering ratios of various polarizations for dry, wet, icy, and snowy asphalt have been found to be sufficiently different road-condition recognition at 24 GHz. The effect of water on the backscattering properties of asphalt has been

studied with experiments and with a surface scattering model. According to laboratory and field experiments, water increases the ratio $\sigma_{\rm vv}/\sigma_{\rm hh}$ by 3–9 dB at large incidence angles, as compared with dry asphalt. The results with the surface scattering model verify that water increases the ratio $\sigma_{\rm vv}/\sigma_{\rm hh}$. The predicted change of 17 dB at 70° incidence, however, was larger than the measured one (7 dB). The surface scattering model has also been used to study how surface parameters affect the backscattering properties of asphalt. It was found that water changes the backscattering properties of asphalt more than there may be differences caused by various asphalt types. Therefore, water can be reliably detected.

The backscattering properties of icy asphalt were studied with laboratory and field experiments. Both experiments showed that contrary to water, which increases the ratio $\sigma_{\rm vv}/\sigma_{\rm hh}$, ice decreases it by 1–2 dB at large incidence angles, as compared with dry asphalt. Field experiments also showed that normalized cross-polarization components, i.e., $\sigma_{\rm vh}/\sigma_{\rm hh}$ and $\sigma_{\rm hv}/\sigma_{\rm hh}$, are 1–2 dB lower with icy asphalt than with dry asphalt. Snow was found to further decrease ratios $\sigma_{\rm vv}/\sigma_{\rm hh}$, $\sigma_{\rm vh}/\sigma_{\rm hh}$, and $\sigma_{\rm hv}/\sigma_{\rm hh}$ by 1–2 dB, as compared with icy asphalt.

A road condition recognition radar needs to be able to measure backscattering for different polarizations. Commercial automotive radars could be modified by adding a dual-polarized antenna with a switch in the transmitter or the receiver side or both. In addition, if using a multipurpose radar, a switchable antenna is required such that the radar beam can be switched between the road surface and the direction of motion of the vehicle. Power budget calculations showed that a 24-GHz short-range radar for road-condition recognition is quite feasible.

ACKNOWLEDGMENT

The authors would like to thank H. Hakojärvi for his help with the field measurements.

REFERENCES

[1] R. Abou-Jaoude, "ACC radar sensor technology, test requirements, and test solutions," *IEEE Trans. Intell. Transp. Syst.*, vol. 4, no. 3, pp. 115–122, Sep. 2003.

[2] *Electromagnetic Compatibility and Radio Spectrum Matters (ERM); Radio Equipment to be Used in 24 GHz Band; System Reference Document for Automotive Collision Warning Short Range Radar*, ETSI TR 101 982 V1.2.1, Jul. 2002.

[3] *Electromagnetic Compatibility and Radio Spectrum Matters (ERM); Road Transport and Traffic Telematics (RTTT); Radar Equipment Operating in the 76 GHz to 77 GHz Range; Part 1: Technical Characteristics and Test Methods for Radar Equipment Operating in the 76 GHz to 77 GHz Range*, ETSI EN 301 091-1 V1.3.3, Nov. 2006.

[4] *Electromagnetic Compatibility and Radio Spectrum Matters (ERM); Road Transport and Traffic Telematics (RTTT); Radio Equipment to be Used in the 77 GHz to 81 GHz Band; System Reference Document for Automotive Collision Warning Short Range Radar*, ETSI TR 102 263 V1.1.2, Feb. 2004.

[5] M. Andersson, F. Bruzelius, J. Casselgren, M. Gäfvert, M. Hjort, J. Hultén, F. Håbring, M. Klomp, G. Olsson, M. Sjödahl, J. Svendenius, S. Woxneryd, and B. Wälivaara, "Road friction estimation," Saab Automobile AB, Trollhättan, Sweden, Jun. 2007. IVSS Project Rep., Ref. no. 2004:17750.

[6] R. Finkele, A. Schreck, and G. Wanielk, "Polarimetric road condition classification and data visualisation," in *Proc. Int. Geosci. Remote Sens. Symp.*, Firenze, Italy, Jul. 1995, pp. 1786–1788.

[7] H. Rudolf, G. Wanielik, and A. J. Sieber, "Road condition recognition using microwaves," in *Proc. IEEE Conf. Intell. Transp. Syst.*, Boston, MA, Nov. 1997, pp. 996–999.

[8] F. T. Ulaby, K. Sarabandi, and A. Nashashibi, "Statistical properties of the Mueller matrix of distributed targets," *Proc. Inst. Elect. Eng.—F*, vol. 139, no. 2, pp. 136–146, Apr. 1992.

[9] R. Kees and J. Detlefsen, "Road surface classification by using a polarimetric coherent radar module at millimetre waves," in *Proc. IEEE Nat. Telesystems Conf.*, 1994, pp. 95–98.

[10] R. Finkele, "Detection of ice layers on road surfaces using a polarimetric millimeter wave sensor at 76 GHz," *Electron. Lett.*, vol. 33, no. 13, pp. 1153–1154, Jun. 1997.

[11] W. Hetzner, "Recognition of road conditions with active and passive millimetre-wave sensors," *Frequenz*, vol. 38, no. 7/8, pp. 179–185, 1984.

[12] G. Magerl, W. Pritzl, and W. Fröhling, "Remote sensing of road condition," in *Proc. Int. Geosci. Remote Sens. Symp.*, Jun. 1991, pp. 2137–2140.

[13] B. Ma, S. Lakshmanan, and A. O. Hero, III, "Simultaneous detection of lane and pavement boundaries using model-based multisensor fusion," *IEEE Trans. Intell. Transp. Syst.*, vol. 1, no. 3, pp. 135–147, Sep. 2000.

[14] S. H. Tsang, P. S. Hall, E. G. Hoare, and N. J. Clarke, "Advance path measurement for automotive radar applications," *IEEE Trans. Intell. Transp. Syst.*, vol. 7, no. 3, pp. 135–147, Sep. 2006.

[15] G. Alessandretti, A. Broggi, and P. Cerri, "Vehicle and guard detection using radar and vision data fusion," *IEEE Trans. Intell. Transp. Syst.*, vol. 8, no. 1, pp. 95–105, Mar. 2007.

[16] A. Eidehall, J. Pohl, F. Gustafsson, and J. Ekmark, "Toward autonomous collision avoidance by steering," *IEEE Trans. Intell. Transp. Syst.*, vol. 8, no. 1, pp. 84–94, Mar. 2007.

[17] R. Schneider, G. Wanielik, and J. Wenger, "Radar arrangement for road condition detection in motor vehicle," German Patent DE 19 715 999, Oct. 1998.

[18] R. Finkele, A. Schreck, and G. Wanielik, "Multi-sensor advance detection of road conditions in front of vehicle using narrow beam millimeter radar and infrared radar beam targeting a road section in front of vehicle," German Patent DE 19 932 094, Jan. 2001.

[19] H. S. Kim, "Road surface sensing device," Korean patent KR 2001 047 234, Jun. 2001.

[20] V. Viikari, T. Varpula, and M. Kantanen, "Automotive radar technology for detecting road conditions. Backscattering properties of dry, wet, and icy asphalt," in *Proc. Eur. Radar Conf.*, 2008, pp. 276–279.

[21] A. K. Fung, *Microwave Scattering and Emission Models and Their Applications*. Boston, MA: Artech House, 1994. 573 p.

[22] [Online]. Available: http://www.clippercontrols.com/info/dielectric_constants.html

[23] [Online]. Available: http://hypertextbook.com/physics/electricity/dielectrics/

[24] T. Meissner and F. J. Wentz, "The complex dielectric constant of pure and sea water from microwave satellite observations," *IEEE Trans. Geosci. Remote Sens.*, vol. 42, no. 9, pp. 1836–1849, Sep. 2004.

[25] M. Wollitzer, J. Buechler, J.-F. Ly, U. Siart, E. Schmidhammer, J. Detlefsen, and M. Esslinger, "Multifunctional radar sensor for automotive application," *IEEE Trans. Microw. Theory Tech.*, vol. 46, no. 5, pp. 701–708, May 1998.

[26] M. Klotz and H. Rohling, "24 GHz radar sensors for automotive applications," in *Proc. 13th Int. Conf. MIKON*, 2000, pp. 359–362.

Ville V. Viikari (S'06–A'09) was born in Espoo, Finland, in 1979. He received the M.Sc. (tech.), Lic.Sc. (tech.) (with distinction), and D.Sc. (tech.) (with distinction) degrees in electrical engineering from the Helsinki University of Technology (TKK), Espoo, in 2004, 2006, and 2007, respectively.

From 2001 to 2007, he was a Trainee, an Assistant Researcher, and a Researcher with the Radio Laboratory, TKK, where he studied antenna measurement techniques at submillimeter wavelengths and antenna pattern-correction techniques. He is currently a Research Scientist with the VTT Technical Research Centre of Finland, Espoo. His current research interests are radio-frequency identification systems and wireless sensors.

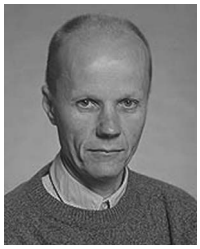

Timo Varpula was born in Seinäjoki, Finland, in 1954. He received the Ph.D. degree in technical physics from the Helsinki University of Technology (TKK), Espoo, Finland, in 1982.

At TKK, he conducted research on weak magnetic fields produced by the human brain, eye, and heart. He also developed superconducting magnetometers and data analysis for biomagnetic signals. He was with the Instrumentarium Corporation Ltd., where he was a Project Manager from 1983 to 1986, developing whole-body nuclear magnetic resonance imaging systems, and a Section Leader from 1986 to 1994, conducting research on measurement devices for metrological and industrial purposes. Since 1994, he has been with the VTT Technical Research Centre of Finland, Espoo, where he was a Group Manager with VTT Automation and VTT Information Technology from 1994 to 2004, was the Research Manager with VTT Microsensing from 2004 to 2006, and is currently a Technology Manager with VTT Sensing and Wireless Devices. He is a coauthor of 45 scientific publications. He is the holder of seven patents. His research interests include radio-frequency (RF) identification, RF, microwave, and wireless sensors for scientific and industrial applications.

Mikko Kantanen received the M.Sc. and Lic.Sc. degrees in electrical engineering from the Helsinki University of Technology (TKK), Espoo, Finland, in 2001 and 2006, respectively.

Since 2001, he has been a Research Scientist with the VTT Technical Research Centre of Finland, Espoo, in the areas of millimeter-wave integrated circuit design, millimeter-wave measurements, and millimeter-wave systems.

Mr. Kantanen is a corecipient of the 2006 Asia-Pacific Microwave Conference Prize.